Journal of Alloys and Compounds 547 (2013) 113–117

Contents lists available at SciVerse ScienceDirect

Journal of Alloys and Compounds

journal homepage: www.elsevier.com/locate/jalcom

One-dimensional WO_3 nanorods as photoelectrodes for dye-sensitized solar cells

Seok-Min Yong, Tsvetkov Nikolay, Byung Tae Ahn, Do Kyung Kim *

Department of Materials Science and Engineering, Korea Advanced Institute of Science and Technology (KAIST), 291 Daehak-ro, Yuseong-gu, Daejeon 305-701, Republic of Korea

ARTICLE INFO

Article history:
Received 15 June 2012
Received in revised form 28 August 2012
Accepted 29 August 2012
Available online 6 September 2012

Keywords:
Dye-sensitized solar cell
Tungsten oxide
One-dimensional nanostructure
Nanorods

ABSTRACT

Tungsten oxide (WO_3) nanorods were applied for the first time as photoelectrodes in dye-sensitized solar cells (DSSCs). The DSSC based on WO_3 nanorods showed a short-circuit current, an open-circuit voltage, a fill factor, and a conversion efficiency of 4.66 mA/cm^2, 0.383 V, 0.22, and 0.75%, respectively. The WO_3 nanorod photoelectrode was treated with $TiCl_4$ aqueous solution to improve the dye absorption and open-circuit voltage by coating the thin TiO_2 layer on the WO_3 nanorod surface. The $TiCl_4$ treatment resulted in the enhanced performance of the short-circuit current of 6.75 mA/cm^2, the open-circuit voltage of 0.457 V, the fill factor of 0.489, and the conversion efficiency of 1.51%. These values can be compared with 5.55 mA/cm^2, 0.447 V, 0.423, and 1.05% for the photoelectrode based on the $TiCl_4$-treated WO_3 nanoparticles. The higher short-circuit current and fill factor for the nanorods compared with the nanoparticles can be attributed to the high charge transport property of the 1-D nanostructure.

1. Introduction

Since O'Regan and Grätzel firstly reported in 1991 [1], dye-sensitized solar cells (DSSCs) have attracted considerable interest as potential candidates to replace conventional Si-based solar cells in specialized applications because of low manufacturing cost and easy fabrication [2,3]. A DSSC is composed as follows (Fig. 1): transparent conducting substrate, mesoporous semiconductor oxide film (photoelectrode), dye molecules absorbed on the surface of oxide surface, electrolyte (iodide/tri-iodide couple), and Pt-coated transparent conducting substrate (counter electrode). When a photon is absorbed by a dye, the excited dye transfers an electron to the conduction band of semiconductor oxide. The oxidized dye is reduced by iodide. The electron in the photoelectrode passes through the external load and reduces tri-iodide to iodide at the counter electrode [2].

TiO_2 are typically used as the photoelectrode and gives the highest efficiency of about 11% [4]. ZnO and SnO_2 have been widely studied as possible alternatives of the TiO_2. ZnO and SnO_2-based DSSCs have been achieved 6.6 [5] and 6.3% [6] efficiencies, respectively. Besides these oxides, Nb_2O_5 [7] and $SrTiO_3$ [8] have been also investigated.

Tungsten oxide (WO_3) is a semiconductor oxide material with a band-gap of 2.6–3.0 eV [9], and it is becoming the focus of research attention due to its unique electronic properties. In particular, various WO_3 nanostructures (nanoparticles, nanoplatelets, nanorods, and nanowires) are of special interest as promising candidates for photocatalyst [9], electrochromic devices [10–12], and gas sensors [13,14] because of their high surface area and novel properties [15]. Recently, Zheng et al. [16] reported for the first time that WO_3 nanostructures have the potential to be used as alternative photoelectrode materials in dye-sensitized solar cells. They used commercial WO_3 nanoparticles with a size of approximately 40 nm as the photoelectrode in DSSC and investigated the effect of various parameters on the cell performance. DSSCs based on WO_3 nanoparticles exhibited a conversion efficiency of 0.75%, which was enhanced up to 1.46% by the surface modification. However, the problem is that the efficiency is relatively lower than that of DSSCs based on the other semiconducting metal oxides, such as TiO_2, SnO_2, and ZnO.

In the last decade, numerous approaches to improving the performance of DSSCs have been considered. Among many possible approaches, introducing a one-dimensional (1-D) nanostructure (nanowires, nanorods, and nanotubes) as the photoelectrode is one of the most promising candidates. In the operational process of DSSC, some electrons in conduction band of the photoelectrode travel back to the electrolyte, which results in a loss of efficiency in the DSSC [2,17]. Therefore, it is important to suppress this recombination reaction and to improve the collection of photo-injected electrons for enhancing the cell performance. The 1-D nanostructures can help to provide a rapid collection of photo-injected electrons because of their outstanding electron transport property [18–20]. Law et al. [21] first introduced a dense array of oriented, crystalline ZnO nanowire instead of the traditional nanoparticle film. Myahkostupov et al. [22] fabricated the DSSCs using hydrothermally prepared TiO_2 nanotubes. Mor et al. [23] prepared highly ordered transparent TiO_2 nanotubes arrays and applied them to the photoelectrode for DSSCs.

* Corresponding author. Tel.: +82 82 42 350 4118; fax: +82 82 42 350 3310.
E-mail address: dkkim@kaist.ac.kr (D.K. Kim).

0925-8388/$ - see front matter © 2012 Elsevier B.V. All rights reserved.
http://dx.doi.org/10.1016/j.jallcom.2012.08.124

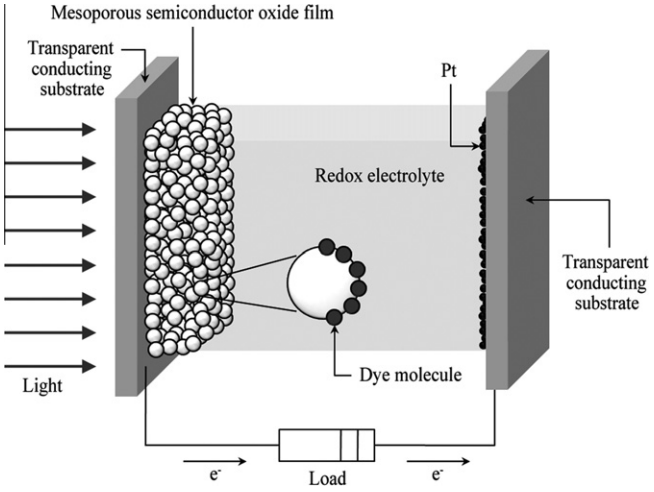

Fig. 1. Schematic diagram of a dye-sensitized solar cell.

In this study, we present for the first time a DSSC based on WO_3 nanorods and investigated the influence of 1-D WO_3 nanostructures on the conversion efficiency enhancement of DSSCs. The effect of surface modification by the $TiCl_4$ treatment was also studied. To the best of our knowledge, this is the first report on the use of 1-D WO_3 nanorods as a photoelectrode for DSSCs.

2. Experimental

The source material of the $W_{18}O_{49}$ nanorods was synthesized following the experimental procedure reported in our group [24]. Initially, the starting solution was prepared by dissolving 8.1 g of tungsten hexachloride in 200 mL of ethanol. Next, 10 mL of starting solution was mixed with 60 mL of ethanol under mild magnetic stirring at room temperature. The final solution was transferred into a 100 mL Teflon-lined stainless steel autoclave, which was sealed and maintained at 200 °C for 10 h in a preheated electric oven and then allowed to cool to room temperature. The products were collected and washed repeatedly with deionized water and ethanol and then dried at 60 °C for 12 h.

The details of the electrode fabrication and DSSC assembly are described elsewhere [25]. A fluorine-doped tin oxide (FTO)-coated glass (7 Ω/cm^2) was sequentially cleaned in acetone, in 0.1 M HCl ethanolic solution, in deionized water, and in ethanol. After cleaning, a $W_{18}O_{49}$ nanorod paste was coated on the FTO glass by the doctor-blade method. The paste was prepared by mixing $W_{18}O_{49}$ nanorods with terpineol and ethyl cellulose ethanol solution. This mixture was then sonicated and stirred for 24 h. Ethanol was removed from this mixture solution by a rotary evaporator. The final paste contained 18 wt.% $W_{18}O_{49}$, 9 wt.% ethyl cellulose, and 73 wt.% terpineol. Finally, the coated film was sintered at 500 °C for 30 min in air; through this sintering process, the phase of $W_{18}O_{49}$ changed to WO_3. Additionally, a $TiCl_4$ treatment was conducted to coat a TiO_2 layer on the WO_3 nanorods. The sintered WO_3 nanorod electrodes were immersed in 40 mM aqueous $TiCl_4$ solution at 70 °C for 1 h, then rinsed with water and ethanol and resintered at 500 °C for 30 min. The thickness of the coated film was measured to be approximately 13 μm.

For the dye coating, the photoelectrodes were dipped in a 0.5 mM N719 dye solution in a mixture of acetonitrile and *tert*-butyl alcohol (1: 1 volume ratio) for 24 h. After the sensitizer uptake, the photoelectrodes were washed with acetonitile. A platinum-coated FTO glass was used as a counter electrode. A Platinum coating was produced by thermal decomposition of H_2PtCl_6. The counter- and photoelectrodes were assembled into the sandwich-type cell and sealed with an ionomer film (Meltonix 1170-60). The internal space of the cell was filled with a liquid electrolyte by capillary action. The commercially available electrolyte AN-50 (Solaronix) was used. The active area of the fabricated cells was varied from 0.14 to 0.16 cm^2.

The phase of the synthesized product was characterized by an X-ray diffractometer (XRD, D/MAX-IIIC, Rigaku, Japan) with Cu Kα radiation. Scanning electron microscopy (SEM, XL30, Philips, Netherlands) and transmission electron microscopy (TEM, JEM-3010, JEOL, Japan) were utilized to observe the morphology and size of the products. The thickness of the film was measured with a surface profile system (Alpha Step 500, Tencor, USA).

The photovoltaic properties of the fabricated cells were measured by recording the current–density–voltage characteristics under illumination with a Polaronix K202 (McScience, Korea) equipped with a 100W Xenon lamp and an AM 1.5G filter set. The incident light intensity was set at 100 mW/cm^2 using a PVM-580 Si reference

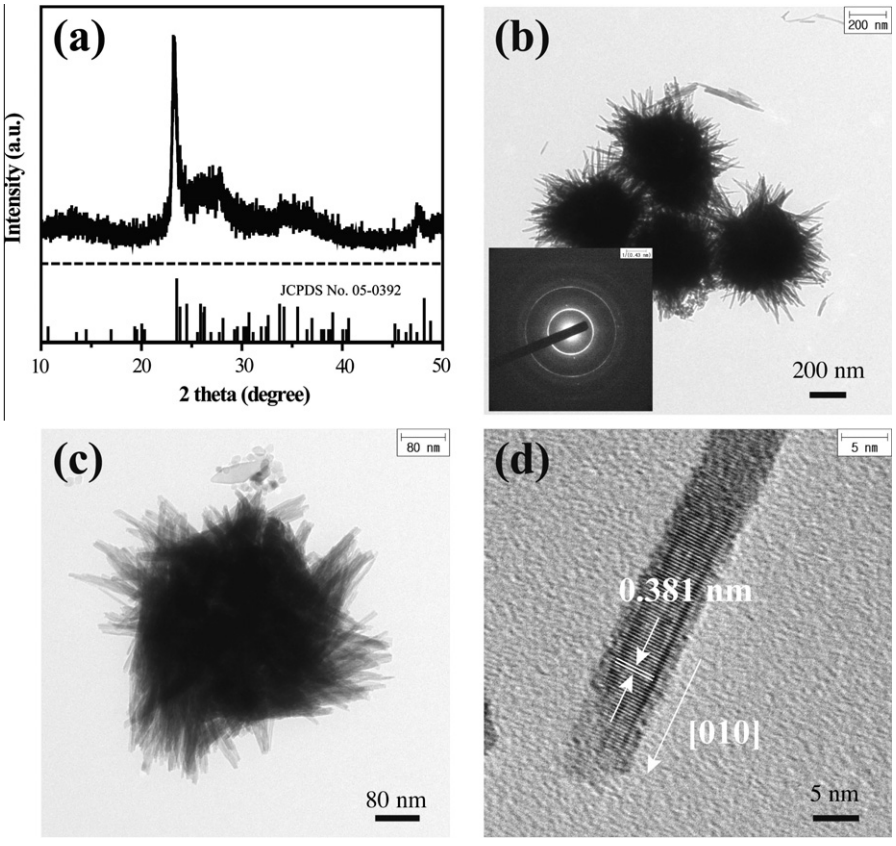

Fig. 2. (a) XRD pattern, (b) and, (c) TEM, and (d) HR-TEM micrographs of the as-synthesized $W_{18}O_{49}$ nanorods. Inset in (b) shows the electron diffraction pattern.

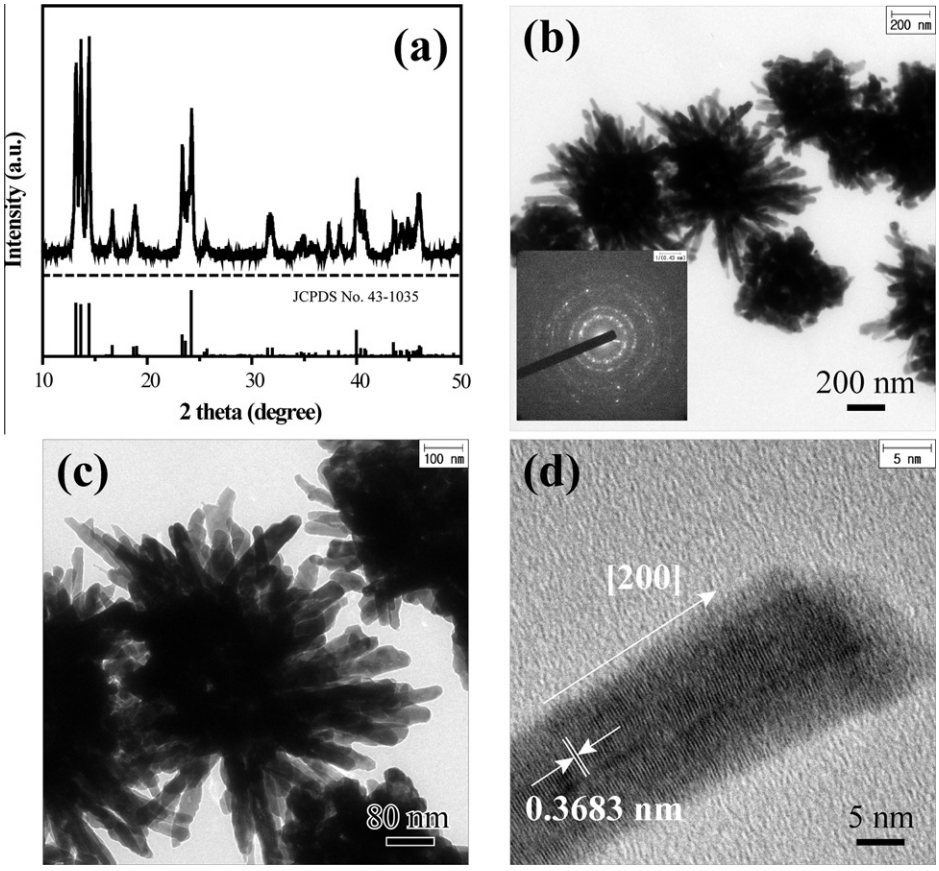

Fig. 3. (a) XRD pattern, (b) and (c) TEM, and (d) HR-TEM micrographs of the WO_3 nanorods obtained by the heat treatment of the $W_{18}O_{49}$ nanorods at 500 °C for 30 min in air. Inset in (b) shows the electron diffraction pattern.

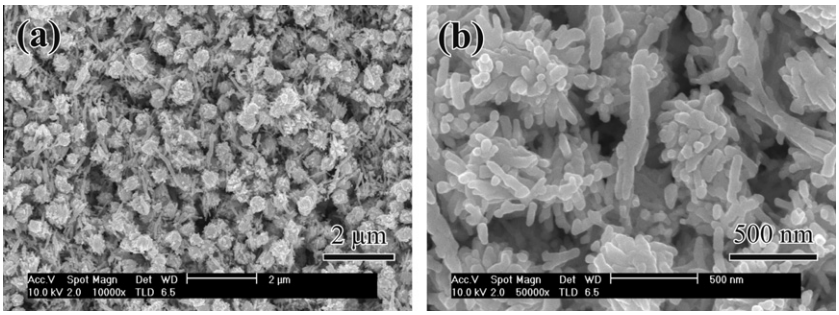

Fig. 4. SEM images of (a) low and (b) high magnification showing the top view of the WO_3 nanorod film.

photodiode (PV Measurements Inc., USA). The current density–voltage curves were recorded by applying an external bias to the solar cell and measuring the photocurrent with a photovoltaic power meter (PolaronixK101/LAB20, McScience, Korea). The incident photon-to-electron conversion efficiency (IPCE) spectra were recorded with a commercial measurement system (QEX7, PV Measurements Inc., USA). The measurements were carried out in an ambient environment.

3. Results and discussion

Fig. 2 displays the XRD pattern, TEM, HR-TEM micrographs, and electron diffraction pattern of the as-synthesized products. Fig. 2(a) shows the XRD pattern of the as-synthesized product, which matched monoclinic $W_{18}O_{49}$ (JCPDS No. 05-0392). As shown in Fig. 2(b) and (c), TEM images show that the as-prepared $W_{18}O_{49}$ sample is assembled in an urchin-like structure consisting of the individual nanorods. The inset indicates an electron diffraction pattern in which all rings could be indexed to the monoclinic phase of $W_{18}O_{49}$. A typical HR-TEM image is shown in Fig. 2(d), which makes it obvious that the individual $W_{18}O_{49}$ nanorods have an average diameter of 7.4 nm and a length of 143 nm. A clearly observed lattice fringe confirms the nanorod is a well-crystallized single crystal. The calculated distance of the interplane perpendicular to the axis direction of the nanorod is 0.381 nm, corresponding to the (0 1 0) lattice spacing of monoclinic $W_{18}O_{49}$. These results are in good agreement with the reported paper [24].

In the process of the DSSC fabrication, sintering of the coated photoelectrode film should be required to improve the interconnection between the nanoparticles and adhesion between the coated films and the FTO glass substrate. The sintering condition was 500 °C for 30 min in air [16,25]. The change of the phase and morphology of $W_{18}O_{49}$ nanorods after the heat treatment was investigated. Fig. 3 displays the XRD pattern, TEM, HRTEM micrographs, and electron diffraction pattern of the $W_{18}O_{49}$ sample

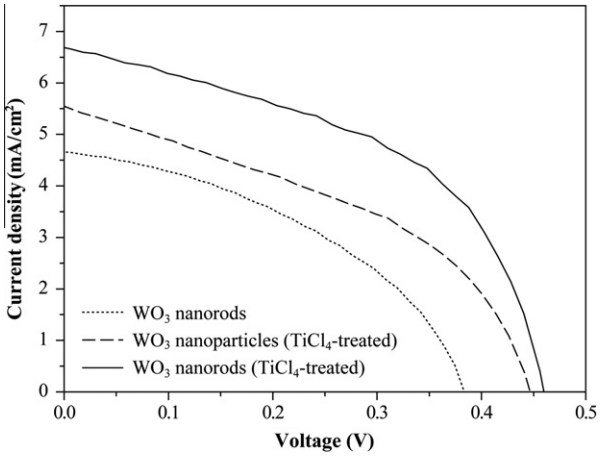

Fig. 5. The current density–voltage (J–V) characteristics of the fabricated DSSCs based on photoelectrodes made of WO_3 nanorods (dotted line), $TiCl_4$-treated WO_3 nanorods (straight line), and $TiCl_4$-treated WO_3 nanoparticles (dashed line).

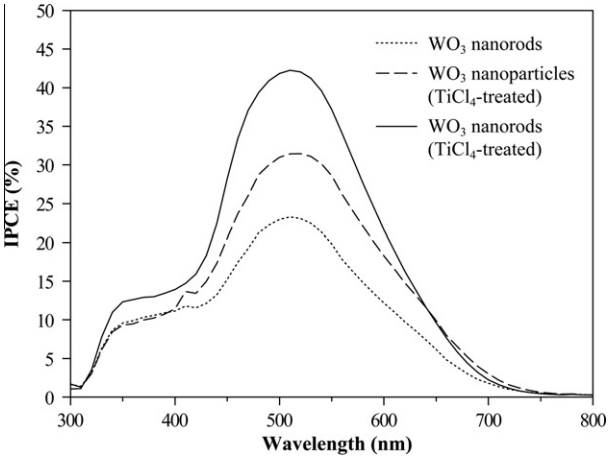

Fig. 6. The incident photon-to-electron conversion efficiency (IPCE) of the fabricated cells based on WO_3 nanorods (dotted line), $TiCl_4$-treated WO_3 nanorods (straight line), and $TiCl_4$-treated WO_3 nanoparticles (dashed line).

Table 1
Performances of the fabricated cells based on WO_3 nanorods and nanoparticles. Each data was the average of five cells.

Photoelectrode type	J_{SC} (mA/cm^2)	V_{OC} (V)	*FF*	η (%)
WO_3 nanorods	4.66 ± 0.50	0.383 ± 0.014	0.422 ± 0.035	0.75 ± 0.06
WO_3 nanoparticles ($TiCl_4$-treated)	5.55 ± 0.16	0.447 ± 0.010	0.423 ± 0.013	1.05 ± 0.02
WO_3 nanorods ($TiCl_4$-treated)	6.75 ± 0.15	0.457 ± 0.016	0.489 ± 0.019	1.51 ± 0.10

treated at 500 °C for 30 min in air. The XRD pattern of the $W_{18}O_{49}$ sample after heat treatment is shown in Fig. 3(a). All the diffraction peaks can be indexed to phase-pure and monoclinic WO_3 (JCPDS No. 43-1035). This XRD result demonstrates that the $W_{18}O_{49}$ phase was oxidized to the WO_3 phase during the heat treatment in air. The color also changed from the dark blue of $W_{18}O_{49}$ to yellow after the heat treatment. Tungsten oxide has various colors for different W/O molar ratio, such as a brown WO_2 phase, a blue suboxide of W, and yellow WO_3 [24]. Therefore, the phase change could be inferred by the change of the powder color after heat treatment.

Fig. 3(b) and (c) show the TEM images of the $W_{18}O_{49}$ sample after heat treatment. It was observed that the morphology (nanorod shape) was maintained, but the diameter increased dramatically. The average diameter is approximately 43 nm compared with the 7.4 nm for the $W_{18}O_{49}$ nanorods. This increase of diameter could be explained by the grain growth that occurred between the contacted nanorods of the assembled structure during the sintering process. The HR-TEM image in Fig. 3(d) shows that the crystal planes perpendicular to the axis direction are separated by 0.3683 nm, which coincides with the (200) plane of monoclinic WO_3. The above results clearly reveal that the $W_{18}O_{49}$ nanorods change into WO_3 nanorods with increased diameter.

Fig. 4(a) and (b) depict the SEM image showing the top view of the WO_3 nanorod film. It was identified that the assembled structure of the nanorods was maintained, although the phase was changed from $W_{18}O_{49}$ to WO_3, and the diameter increased approximately sixfold. It was also confirmed that a film with a porous structure was successfully fabricated. The porosity of the film is an important factor because a large surface-to-volume ratio means an increase of dye absorption, which then facilitates the photocurrent enhancement.

Fig. 5 exhibits the current density–voltage (J–V) characteristics of the fabricated DSSCs based on photoelectrodes made of WO_3 nanorods and nanoparticles. The value of the open circuit voltage (V_{OC}), the short-circuit current density (J_{SC}), the fill factor (*FF*), and the conversion efficiency (η) are also summarized in Table 1. Each data was the average of five cells. A DSSC based on WO_3 nanorods showed J_{SC} = 4.66 mA/cm^2, V_{OC} = 0.383 V, *FF* = 0.422, and η = 0.75% (dotted line). All values are relatively lower than those of conventional DSSCs based on TiO_2 nanoparticles. The V_{OC} of a DSSC is determined by the difference between the Fermi level of the photoelectrode and the redox potential of the electrolyte [2]. WO_3 has −0.4 V versus NHE for I^-/I_3^- electrolyte [16]; thus, it could be predicted that the V_{OC} of the WO_3-based DSSC is on the order of 0.4 V, which is in good agreement with our V_{OC} result (0.383 V). The lower J_{SC} and *FF* are mainly attributed to a low isoelectric point (ISP) of WO_3. The ISP is simply the pH value at which the metal oxide surface carries no net electric charge [26]. The ISP of WO_3 is pH = 0.4–1 [27], which means that the WO_3 surface is negatively charged in the dye solution. Therefore, dye absorption on the WO_3 surface is poor because the anchoring ligand of the N719 dye is the negatively charged carboxylic group [2,16]. The low dye loading results in the restriction of excited electron quantities and an increase of the dark current by the direct contact between the electrolyte and the WO_3 photoelectrode.

Meanwhile, it has been reported that TiO_2 coating on the SnO_2 improved the cell performance by minimizing the problems of insufficient dye attachment and low V_{OC} [5]. Similarly, to enhance the performance of WO_3-based DSSCs, an ultrathin TiO_2 layer coating on the WO_3 surface was deposited by a $TiCl_4$ treatment, as mentioned in the Section 2. As shown in Fig. 5 (straight line) and Table 1, the DSSC based on the $TiCl_4$-treated WO_3 nanorods exhibited the cell performance of J_{SC} = 6.75 mA/cm^2, V_{OC} = 0.457 V, *FF* = 0.489, and η = 1.51%, all higher than the values of the DSSC based on WO_3 nanorods. Several factors could contribute to performance enhancement. First, the dye absorption on the WO_3 surface increases because the TiO_2 has the higher ISP of pH = 5.9–6.0 [16,28], resulting in the improvement of J_{SC} and *FF*. Second, TiO_2 acts as a barrier layer to suppress the electron interception by the electrolyte, which enhances the J_{SC}, V_{OC}, and *FF*. Third, the conduction band of WO_3 is negatively shifted by the TiO_2 layer because the TiO_2 has the higher conduction band than WO_3, which provides the enhancement of V_{OC} [3,17].

The effect of the 1-D WO_3 morphology on the cell performance was also investigated. A DSSC based on $TiCl_4$-treated WO_3 nanoparticles (Aldrich, size ~ 40 nm) was fabricated, and the cell performance was tested. The DSSC based on $TiCl_4$-treated WO_3

nanoparticles showed the performance of the J_{SC} = 5.55 mA/cm^2, V_{OC} = 0.447 V, FF = 0.423, and η = 1.05% (Fig. 5, dashed line). It was found that the DSSC based on $TiCl_4$-treated WO_3 nanorods exhibited a higher J_{SC} and FF than the DSSC based on $TiCl_4$-treated WO_3 nanoparticles. This means that the electron transport in the 1-D nanorods is fairly faster than percolation through nanoparticle network, which contribute to reduction of the charge recombination.

Fig. 6 shows the incident photon-to-electron conversion efficiency (IPCE), or "quantum efficiency (QE)" of the fabricated cells based on $TiCl_4$-treated WO_3 nanorods and nanoparticles. The IPCE results support the increase of J_{SC} from the $TiCl_4$ treatment and the adoption of a 1-D nanostructure.

4. Conclusion

Tungsten oxide (WO_3) nanorods were introduced for the first time as a photoelectrode in DSSCs. The WO_3 nanorod photoelectrode was obtained through the sintering process of the $W_{18}O_{49}$ nanorod film. During the sintering process, the $W_{18}O_{49}$ was oxidized to WO_3 and the diameter of nanorods increased from 7.4 to 43 nm. The fabricated DSSC based on WO_3 nanorods showed a short-circuit current density (J_{SC}) of 4.66 mA/cm^2, an open-circuit voltage (V_{OC}) of 0.383 V, a fill factor (FF) of 0.422, and a conversion efficiency (η) of 0.75%. $TiCl_4$ treatment of the WO_3 nanorod photoelectrode was carried out to overcome the problems of low dye-loading and V_{OC} by coating the TiO_2 on the WO_3 nanorod surface. As a result, a significant improvement of the cell performance was achieved; J_{SC} = 6.75 mA/cm^2, V_{OC} = 0.457 V, FF = 0.489, and η = 1.51%. This enhancement is attributed to the increase of dye loading, the suppression of recombination reaction, and the negatively shift of the conduction band by TiO_2 coating. To investigate the effect of the 1-D morphology on the cell performance, a DSSC based on $TiCl_4$-treated WO_3 nanoparticles with a size of 40 nm was fabricated and characterized. The DSSC based on $TiCl_4$-treated WO_3 nanoparticles exhibited the performance of J_{SC} = 5.55 mA/cm^2, V_{OC} = 0.447 V, FF = 0.423, and η = 1.05%. The nanorods showed a higher J_{SC} and FF than the nanoparticles, which could be primarily due to the efficient electron transfer through the 1-D nanostructures. These results reveal that the 1-D WO_3 nanostructure is a promising photoelectrode material for DSSCs. In comparison with the conventional TiO_2-based DSSCs, however, the conversion efficiency of WO_3-based DSSCs is still low. It is expected that the conversion efficiency of WO_3-based DSSCs can be enhanced by introducing the blocking layer to suppress the recombination reaction from FTO to electrolyte [25,29], and fabricating the photoelectrode with high surface area for higher dye loading and light harvesting [30,31].

Acknowledgements

This work was supported by Priority Research Centers Program (2011-0031407), the Pioneer Research Center Program (2010-0019469), and Program to Solve Climate Changes (NRF-2010-C1AAA001-2010-0029031) through the National Research Foundation of Korea (NRF) funded by the Ministry of Education, Science and Technology.

References

[1] B. Oregan, M. Gratzel, Nature 353 (1991) 737–740.
[2] A. Hagfeldt, G. Boschloo, L.C. Sun, L. Kloo, H. Pettersson, Chem. Rev. 110 (2010) 6595–6663.
[3] C. Prasittichai, J.T. Hupp, J. Phys. Chem. Lett. 1 (2010) 1611–1615.
[4] Y. Chiba, A. Islam, Y. Watanabe, R. Komiya, N. Koide, L.Y. Han, Jpn. J. Appl. Phys. 45 (2006) L638–L640.
[5] A. Kay, M. Gratzel, Chem. Mater. 14 (2002) 2930–2935.
[6] M. Saito, S. Fujihara, Energy Environ. Sci. 1 (2008) 280–283.
[7] P. Guo, M.A. Aegerter, Thin Solid Films 351 (1999) 290–294.
[8] J. Bandara, H.C. Weerasinghe, Sol. Energy Mater. Sol. Cells 88 (2005) 341–350.
[9] F.G. Wang, C. Di Valentin, G. Pacchioni, Chemcatchem 4 (2012) 476–478.
[10] S.K. Deb, Sol. Energy Mater. Sol. Cells 92 (2008) 245–258.
[11] S.J. Yoo, Y.H. Jung, J.W. Lim, H.G. Choi, D.K. Kim, Y.E. Sung, Sol. Energy Mater. Sol. Cells 92 (2008) 179–183.
[12] H.S. Shim, J.W. Kim, Y.E. Sung, W.B. Kim, Sol. Energy Mater. Sol. Cells 93 (2009) 2062–2068.
[13] J.L. Solis, S. Saukko, L. Kish, C.G. Granqvist, V. Lantto, Thin Solid Films 391 (2001) 255–260.
[14] X.L. Li, T.J. Lou, X.M. Sun, Y.D. Li, Inorg. Chem. 43 (2004) 5442–5449.
[15] J.H. Ha, P. Muralidharan, D.K. Kim, J. Alloys Comp. 475 (2009) 446–451.
[16] H.D. Zheng, Y. Tachibana, K. Kalantar-zadeh, Langmuir 26 (2010) 19148–19152.
[17] J.S. Im, S.K. Lee, Y.S. Lee, Appl. Surf. Sci. 257 (2011) 2164–2169.
[18] Y.N. Xia, P.D. Yang, Y.G. Sun, Y.Y. Wu, B. Mayers, B. Gates, Y.D. Yin, F. Kim, Y.Q. Yan, Adv. Mater. 15 (2003) 353–389.
[19] D.K. Kim, P. Muralidharan, H.W. Lee, R. Ruffo, Y. Yang, C.K. Chan, H. Peng, R.A. Huggins, Y. Cui, Nano Lett. 8 (2008) 3948–3952.
[20] S.M. Yong, P. Muralidharan, S.H. Jo, D.K. Kim, Mater. Lett. 64 (2010) 1551–1554.
[21] M. Law, L.E. Greene, J.C. Johnson, R. Saykally, P.D. Yang, Nat. Mater. 4 (2005) 455–459.
[22] M. Myahkostupov, M. Zamkov, F.N. Castellano, Energy Environ. Sci. 4 (2011) 998–1010.
[23] G.K. Mor, K. Shankar, M. Paulose, O.K. Varghese, C.A. Grimes, Nano Lett. 6 (2006) 215–218.
[24] H.G. Choi, Y.H. Jung, D.K. Kim, J. Am. Ceram. Soc. 88 (2005) 1684–1686.
[25] S. Ito, T.N. Murakami, P. Comte, P. Liska, C. Gratzel, M.K. Nazeeruddin, M. Gratzel, Thin Solid Films 516 (2008) 4613–4619.
[26] A. Annamalai, Y.D. Eo, C. Im, M.J. Lee, Mater. Charact. 62 (2011) 1007–1015.
[27] M. Anik, T. Cansizoglu, J. Appl. Electrochem. 36 (2006) 603–608.
[28] S. Pazokifard, S.M. Mirabedini, M. Esfandeh, M. Mohseni, Z. Ranjbar, Surf. Interface Anal. 44 (2012) 41–47.
[29] S. Ito, P. Liska, P. Comte, R.L. Charvet, P. Pechy, U. Bach, L. SchmidtMende, S.M. Zakeeruddin, A. Kay, M.K. Nazeeruddin, M. Gratzel, Chem. Commun. (2005) 4351–4353.
[30] S.H. Ko, D. Lee, H.W. Kang, K.H. Nam, J.Y. Yeo, S.J. Hong, C.P. Grigoropoulos, H.J. Sung, Nano Lett. 11 (2011) 666–671.
[31] M. Zukalova, A. Zukal, L. Kavan, M.K. Nazeeruddin, P. Liska, M. Gratzel, Nano Lett. 5 (2005) 1789–1792.